Determination of Metabolic Fluxes by Deep Learning of Isotope Labeling Patterns

Richard C. Law[1], Samantha O'Keeffe[1], Glenn Nurwono[2], Rachel Ki[3], Aliya Lakhani[1], Pin-Kuang Lai[4], and Junyoung O. Park[1,5*]

[1] Department of Chemical and Biomolecular Engineering, University of California, Los Angeles, Los Angeles, CA 90095

[2] Department of Chemistry and Biochemistry, University of California, Los Angeles, Los Angeles, CA 90095

[3] Department of Statistics and Data Science, University of California, Los Angeles, Los Angeles, CA 90095

[4] Department of Chemical Engineering and Materials Science, Stevens Institute of Technology, Hoboken, NJ 07030

[5] California NanoSystems Institute and Jonsson Comprehensive Cancer Center at UCLA, Los Angeles, CA 90095

* Correspondence: jop@ucla.edu

Abstract

Fluxomics offers a direct readout of metabolic state but relies on indirect measurement. Stable isotope tracers imprint flux-dependent isotope labeling patterns on metabolites we measure; however, the relationship between labeling patterns and fluxes remains elusive. Here we innovate a two-stage machine learning framework termed ML-Flux that streamlines metabolic flux quantitation from isotope tracing. We train machine learning models by simulating atom transitions across five universal metabolic models starting from 26 ^{13}C-glucose, ^{2}H-glucose, and ^{13}C-glutamine tracers within feasible flux space. ML-Flux employs deep-learning-based imputation to take variable measurements of labeling patterns as input and successive neural networks to convert the ensuing comprehensive labeling information into metabolic fluxes. Using ML-Flux with multi-isotope tracing, we obtain fluxes through central carbon metabolism that are comparable to those from a least-squares method but orders-of-magnitude faster. ML-Flux is deployed as a webtool to expand the accessibility of metabolic flux quantitation and afford actionable information on metabolism.

Introduction

Metabolism is a dynamic network of biochemical reactions that support proliferation, differentiation, homeostasis, and biological functions[1]. Metabolic fluxes represent the rates at which organisms operate different metabolic pathways. The culmination of biochemical knowledgebase[2–4], analytical chemistry[5,6], and mathematical modeling[7–9] has established metabolic fluxes as a fundamental descriptor of metabolic state in health and biotechnology[10].

While metabolic fluxes are a direct indicator of the dynamic state of metabolism, they are difficult to measure because rates are intangible quantities. This challenge has become increasingly surmountable thanks to the advent and the development of isotope-based metabolic flux analysis (MFA)[11–14]. As carbon forms the backbone of metabolites and biomass precursors, tracing the fate of ^{13}C from a ^{13}C-labeled substrate to downstream metabolites reveals metabolic pathway utilization[15]. The accuracy of ^{13}C-MFA relies on the use of cleverly chosen tracers and the measurement of isotope labeling patterns of metabolites in convergent pathways. Using nuclear magnetic resonance spectroscopy (NMR)[16] or mass spectrometry (MS)[17,18] measurement of metabolite labeling patterns and mathematical optimization, ^{13}C-MFA searches for fluxes that simulate labeling patterns most consistent with experimental measurements. ^{13}C-MFA tools have increased the adoption of isotope tracing in metabolism research[19–22].

Despite the utility, ^{13}C-MFA remains an expert method due to the need for judicious isotope tracer selection and custom metabolic model building as well as increasing computational costs with larger metabolic networks. To overcome these shortfalls, a simple mathematical function that accepts isotope labeling patterns as input and computes metabolic fluxes as output is needed. Furthermore, for this function to be widely applicable, it needs to take in variable isotope labeling patterns measured by different researchers studying widely divergent biological systems using different analytical instruments.

Here, we create the labeling-to-flux function by combining imputation and deep learning[19]. Artificial neural networks (ANNs) are the epitome of machine learning models with artificial neurons (nodes) whose input signals are transformed into output signals via synapse-like connections (edges)[23]. Partial convolutional neural networks (PCNN) further employ convolution filters and binary masks to learn and impute missing data from experimental measurements (*cf.* inpaint missing pixels/elements in images/matrices)[24]. To streamline this workflow, isotope labeling patterns can be transformed into a matrix as stacked mass isotopomer distribution (MID) vectors for individual metabolites.

Integrating the ANN and PCNN architectures, we developed ML-Flux, a machine-learning-based flux quantitation framework that curtails the model-building process and streamlines the determination of metabolic fluxes. To build ML-Flux, we assembled two categories of models: *i*) metabolic models that encompass biochemical reaction networks with atom mapping; and *ii*) machine learning (ML) models that link characteristic isotope labeling patterns to metabolic flux distributions. For the former, we developed five universal models of central carbon metabolism and generated over a million simulations of isotope labeling patterns from fluxes randomly sampled from feasible flux space. For the latter, we used the resulting data to train, validate, and test ML models for imputing incomplete MIDs and determining fluxes.

Using ML-Flux with data from multi-isotope tracing experiments, we demonstrated three beneficial predictive capabilities: ML-Flux imputed the labeling patterns of unmeasured metabolites (e.g., due to low abundance or stability); ML-Flux inferred the isotope labeling patterns in alternative tracer experiments; and ML-Flux revealed metabolic fluxes similar to those from ^{13}C-MFA that uses a least-squares method. A major advantage of ML-Flux over the traditional MFA method was its speed. ML-Flux quantified metabolic fluxes across divergent organisms ranging from microorganisms and mammalian cells within seconds. We

deployed ML-Flux as a light webtool. The increased accessibility to metabolic flux quantitation will benefit metabolic engineering and metabolic disease research communities.

Results

Fluxes create characteristic isotope labeling patterns

Our ability to quantify metabolic fluxes by isotope tracing relies on deciphering the relationship between metabolic fluxes and corresponding isotope labeling patterns. Tracing atoms from an isotope tracer (e.g., [1,2-$^{13}C_2$]glucose) through metabolic reactions (e.g., glycolytic reactions), one can infer the isotope labeling patterns of downstream metabolites (**Fig. 1a**). Given relative fluxes between two convergent pathways (e.g., upper glycolysis and pentose phosphate pathway, PPP), one can compute the labeling pattern of a metabolite (e.g., glyceraldehyde-3-phosphate, GAP) at the merge point by linear combination (**Fig. 1a**). Therefore, simulating isotope labeling patterns from metabolic fluxes involves straightforward linear algebra (**Fig. 1b**).

The inverse function that maps isotope labeling patterns to metabolic fluxes is nonlinear and convoluted (**Fig. 1b**). For a simplified three-atom network, mimicking upper glycolysis and the pentose phosphate pathway[11], that contains two free net flux and one exchange flux (**Fig. 1c**), we obtained an analytical solution to the fluxes by imposing steady-state mass balance on the isotopomers:

$$\frac{v_{2,r}}{v_1} = \frac{1 - B_{M+1}}{B_{M+1} - D_{M+1}}$$

$$\frac{v_3}{v_1} = \frac{1 - D_{M+1}}{2B_{M+1} - D_{M+1}}$$

B_{M+1} and D_{M+1} are the fractions of the M+1 isotopologues of B and D. These solutions showed that fluxes are functions of isotope labeling patterns and that labeling patterns are characteristic of underlying fluxes (**Fig. 1d**).

Neural networks predict fluxes from labeling patterns

To demonstrate that characteristic labeling patterns can be taught, we trained an ANN model with simulated labeling data using the same simple metabolic model and the [1-$^{13}C_1$]-A tracer (**Fig. 1e**). We sampled fluxes from multiple distributions to determine the best dataset for training an accurate solution (**Extended Data Fig. 1a,b**). The best ANN model orthogonally mapped the labeling-to-flux relationship nearly identically to the analytical solution (**Fig. 1f**).

The task of finding labeling-to-flux functions becomes increasingly challenging as the number of reactions and atoms in the metabolic network increases and as the number of isotope tracers increases. For more complex metabolic networks, we were curious if labeling patterns characteristic of metabolic fluxes could still be taught. We developed models for upper and full glycolysis, glycolysis and the PPP, and central carbon metabolism (CCM) (**Fig. 2a**). To obtain training data, we simulated labeling patterns starting from 24 commercially available ^{13}C-glucose tracers, [5-$^{2}H_1$]-glucose, and the combinations of ^{13}C-labeled and unlabeled glucose and glutamine (**Supplementary Table 1**). For the simple model (**Fig. 1c**), we simulated labeling patterns starting from all six nontrivial isotope tracers (i.e., all combinations of labeled and

unlabeled carbons except the uniformly labeled and the uniformly unlabeled molecules). We trained five ANNs for the prediction of the free fluxes from the isotope labeling patterns (MIDs) of all metabolites (**Extended Data Fig. 2a,b**). Full fluxes were obtained by multiplying free fluxes by the basis of the null space of the stoichiometric matrix representing the metabolic network.

We quantified the accuracy of flux predictions by the ANN models. In the simple model, both free net and exchange fluxes were predicted within 5% error across all testing data (**Fig. 2b**). In the glycolysis models, the flux predictions were within 10% from test data for the exchange fluxes in upper glycolytic reactions. Exchange fluxes in lower glycolytic reactions had interquartile ranges of ±~10% deviation from test data. For the larger metabolic models, which have many net and exchange fluxes, we assessed their ANN model performances by plotting the distribution of mean errors of fluxes (**Fig. 2c**). We observed that the mean error distributions were centered around zero across all fluxes, demonstrating that flux predictions were unbiased. The majority of fluxes had a mean error of less than 0.1 flux unit (normalized to glucose uptake). Noticeably less accurate predictions included exchange fluxes in the non-oxidative PPP and fluxes related to pyruvate cycling. Nonetheless, the trained ANN models demonstrated that, despite its complexity, the underlying relationship between isotope labeling patterns and metabolic fluxes can be learned.

Imputation enables flexible input of labeling patterns into ANN

The obstacle between the development and the widespread adoption of ANN models for flux analysis exists in the labeling pattern input data. The ANN architecture requires a uniform input size (i.e., the labeling patterns of the full set or a fixed subset of metabolites in a metabolic model), whereas the user obtains variable metabolite measurements depending on analyte abundance, stability, environment, and instrumentation. Furthermore, experimentalists may employ various tracers that harbor isotopes at different positions[25–27]. We sought to bridge the gap between experimental measurement and ANN input by imputation of the labeling patterns of the full metabolite set from a comprehensive list of available isotope tracers. To this end, we employed K-nearest neighbors (KNN) regression to predict the labeling of unmeasured metabolites.

KNN regression is a supervised learning algorithm that identifies the K nearest data points from the training data to interpolate the missing values from user data. To test the KNN approach, we generated partially masked labeling patterns that mimic typical experiments with incomplete labeling measurements. Missing labeling values in the MID vector were imputed by the Euclidean distance-weighted average of known values from its three nearest neighbors (K=3) in the complement set of labeling pattern simulations (**Fig. 3a**). As a whole, the distribution of mean absolute errors showed that predicted labeling fractions were less than 0.01 away from the labeling fractions that had been masked for the simple and glycolysis models and less than 0.0005 for the larger two models (**Fig. 3b**). The magnitude of these errors was comparable to that of LC-MS measurement[28]. As the average distance of neighbors increased, we found larger errors between the predicted and actual values; however, KNN regression consistently outputted highly accurate predictions of missing labeling patterns.

Inpainting expedites imputation of unknown labeling patterns

Despite the accuracy of the KNN approach, its computation time became increasingly longer for larger metabolic models. To overcome KNN regression's limitation of imputation speed in large metabolic models, we adopted a PCNN-based inpainting method that is used for restoring missing regions of images. In it, images are processed through convolution filters and random binary masks to train a ML model so it may verisimilarly fill in irregular missing regions of images (**Extended Data Fig. 3**). Since labeling fractions take values between 0 and 1 analogous to grayscale pixels in black and white images, we postulated that the

inpainting process can fill in the matrix of stacked MIDs containing the isotope labeling patterns of measured metabolites and missing values corresponding to unmeasured metabolites (**Fig. 4a**).

To train the PCNN inpainting model, we sampled manifold labeling patterns from physiologically feasible fluxes and the 26 stable isotope tracers of glucose and glutamine and generated binary masks that expose the labeling patterns for a random subset of metabolites from one randomly chosen isotope tracer at a time. To test the plausibility of inpainted labeling pattern matrices, we developed a simple metric ΔN, the difference between the grand sum of the inpainted MID matrix and the total number of measured metabolite instances, since the sum of the labeling fractions (i.e., the values of the MID vector) for a metabolite should be 1. As ΔN approaches 0, plausibility increases. The trained PCNN inpainting model resulted in not only highly plausible predictions but also mean absolute errors less than 0.02 (**Fig. 4b**). A major benefit of the PCNN approach was its computational speed that was invariant with respect to the complexity of the underlying metabolic networks (**Fig. 4c**).

Integrated ML models streamline quantitation of metabolic fluxes

We combined the PCNN and ANN models to convert variable input metabolite labeling measurements to a quantitative metabolic flux map (**Fig. 5a**). The PCNN model determines a full labeling set from incomplete data provided as in real-world isotope tracing experiments. The ANN model uses this output (i.e., the labeling patterns of all metabolites and tracer experiments) to predict the free fluxes. Using linear algebra, the free fluxes engender the full flux distribution.

While the PCNN and ANN predictions of full labeling set and free fluxes, respectively, were accurate as a whole (**Figs. 3** and **4**), the integration of these steps can result in inaccurate predictions. To quantify the compounding effect of the two-stage ML predictions, we plotted the distribution of absolute percent errors for each predicted flux in the simple, upper glycolysis, and full glycolysis models with 40-95% of labeling data masked (**Fig. 5b**). While the median error of the PGI exchange reaction rose from 2% to 20% in the glycolysis model, the TPI exchange reaction was less affected by the inpainted label measurements, increasing from 3% to 8%. The wider range of errors for fluxes from inpainted labels demonstrated the tradeoff between flexible input labeling data (including the choice of tracers) and the accuracy of predicted fluxes. The results also recapitulated the importance of the synergy between [1,2-$^{13}C_2$]- and [5-$^{2}H_1$]-glucose tracers to resolve exchange fluxes in lower glycolysis[28].

In glycolysis+PPP and CCM models, two-stage ML predictions starting from incomplete labeling measurements (with >97% of labeling data masked) reduced the number of accurately predicted (<10% error) fluxes, and errors increased by up to 20% (**Fig. 5c**). CCM flux predictions were less affected by the completeness of the input labeling data (**Extended Data Fig. 4**). Across the five models tested, the computation time for ML-Flux was invariant with respect to model complexity, whereas the computation time for the least-squares method increased as the number of free fluxes in the metabolic model increased (**Fig. 5d**). Taken together, these results highlighted two important lessons: 1) measurement of more metabolites improves the resolution of flux prediction; and 2) not all isotope tracing experiments are equally informative.

ML-Flux turns real-world metabolomics data into accurate fluxes

We evaluated the performance of ML-Flux using real-world metabolomics data. We had previously quantified metabolic fluxes in mammalian cells using [U-$^{13}C_6$]-glucose, [1,2-$^{13}C_2$]-glucose, and [U-$^{13}C_5$]-glutamine and least-squares-based ^{13}C-MFA[28]. We tested if ML-Flux could obtain similar results to the coherent flux set obtained by ^{13}C-MFA using the same data from these tracing experiments, where each

experiment provided different information with regards to fluxes (**Fig. 6a**). We prepared seven different combinations of labeling data (from one, two, or all three tracers) as inputs to ML-Flux and obtained flux predictions. Each tracer excelled at accurately predicting fluxes for a different pathway. In the PPP, [1,2-$^{13}C_2$]-glucose labeling data resulted in flux predictions within 0.303 flux units (normalized to glucose uptake) compared to the ^{13}C-MFA result (**Fig. 6b**). In the tricarboxylic acid (TCA) cycle, flux predictions using the labeling data from [U-$^{13}C_5$]-glutamine tracing were within 0.05 normalized flux units of MFA predictions while the use of other tracers resulted in flux predictions with a larger departure from the MFA ones (**Fig. 6c**). While each tracer was specialized in a subset of central carbon metabolism pathways, ranking the similarity of all predicted fluxes to MFA predictions demonstrated an overall synergistic nature of using multiple tracers to comprehensively resolve pathway fluxes (**Fig. 6d** and **Extended Data Fig. 5**).

ML-Flux webtool increases the accessibility of metabolic flux quantitation

Compared to traditional MFA software, ML-Flux requires little computational resources. Instead of iterative simulation of metabolic models and gradient-descent-based minimization of residuals, ML-Flux uses pre-trained models with the majority computational demand frontloaded in the form of neural network training. As a result, we were able deploy ML-Flux online, creating the first webtool for metabolic flux analysis (**Fig. 6e**). We host ML-Flux and provide documentation and example data on metabolicflux.org to allow researchers to streamline the interpretation of isotope labeling data and metabolic flux quantitation. The ML-Flux software will be regularly updated to incorporate new metabolic models and increase the speed and accuracy of flux quantitation.

Discussion

Metabolic fluxes are determined by the interaction of enzymes and metabolites, which serve as substrates, products, and effectors. Thermodynamic and kinetic rate laws link metabolomics and proteomics to fluxomics[29–31]. The advancement of analytical tools has increased the sensitivity and coverage of metabolite and protein measurement. In this work, we advanced fluxomics by innovating machine learning approaches.

Metabolic flux quantitation relies on our ability to decipher the relationship between isotope labeling patterns imprinted in metabolites and the underlying metabolic fluxes. In simple metabolic networks at (pseudo)steady state, the relationship appears algebraically straightforward by applying mass balance to individual isotopologues[32]. Increasing complexity of metabolic networks renders labeling-flux relationship nearly incomprehensible to human cognition. By training machine learning models with copious labeling-flux pairs sampled from a physiologically relevant flux space, ML-Flux captured inconspicuous labeling-to-flux relationships.

A major challenge in training ANN models for flux prediction was the limited availability of flux measurements in the literature. Currently, the majority of available flux data come from ^{13}C-MFA, which searches for fluxes that the best simulate data based on known atom transitions in known biochemical networks. To overcome this challenge, we generated expansive isotope tracing simulations across central carbon metabolism. Our simulations employed elementary metabolite units[11] (EMU) to quickly and accurately pair metabolic fluxes to corresponding isotope labeling patterns. Therefore, ML-Flux effectively frontloads computational tasks, which for MFA are performed during the least-squares fitting process. Since

ML-Flux obviates ethe need for iterative simulations during flux computation, researchers can now obtain fluxes quickly and easily using MLML-Flux, which we implemented as a light webtool.

Unlike typical ML programs, which require fixed input sizes, ML-Flux allows flexible input sizes to accommodate varying scope of metabolite measurement from diverse isotope tracers. We accomplished this feat by training our ANN models using a comprehensive set of commercially available isotope tracers and incorporating PCNN for imputation of metabolite labeling patterns that are not or cannot be measured. Although the imputation step adds to possibility for potentially erroneous predictions, the PCNN-ANN integrated ML system gave rise to a flux prediction framework that is robust for nearly all conceivable isotope tracing in central carbon metabolism.

Our evaluation of ML-Flux showed that fluxes are predicted with high accuracy for reaction steps that are responsible for creating characteristic labeling patterns with a given tracer. For example, [1,2-$^{13}C_2$]-glucose was useful for determining upper glycolysis and PPP fluxes, whereas [U-$^{13}C_6$]-glucose or [U-$^{13}C_5$]-glutamine was not. We also learned that measurement of the labeling patterns of key metabolites increases the accuracy of flux predictions and that measurement of more metabolites leads to increased resolution of flux predictions. For instance, predicting the exchange fluxes of individual lower glycolytic reactions becomes increasingly erroneous with missing metabolite measurement although we can still predict fluxes reasonably well for lumped reactions that effectively ignore it in the less detailed metabolic model[1]. Therefore, an added benefit of ML-Flux is its ability to impart intuition for labeling-to-flux relationship and informative tracer design.

Traditional metabolic flux analysis focuses on quantifying net fluxes. ML-Flux advances metabolic flux analysis by streamlining the quantification of both net and exchange fluxes. Knowledge of net and exchange fluxes reveals forward and reverse fluxes. The ratio of forward to reverse fluxes reveal reaction reversibility, which is related to Gibbs free energy of reaction based on how close to equilibrium a reaction is by a thermodynamic principle[33]. Furthermore, the ratio of net to total flux (i.e., the sum of forward and reverse fluxes) indicates how efficiently cells utilize enzymes[28]. Therefore, the advancement of flux quantitation by ML-Flux imparts uniquely valuable information on thermodynamics and efficiency of metabolism.

ML-Flux provides dual benefits of streamlining flux quantitation for researchers who are new to fluxomics and producing a sound starting point for the least-squares-based MFA for experienced researchers. ML-Flux complements traditional MFA approaches and bolsters efforts toward adding fluxomics to integrative omic analysis. Thus, the upshot of ML-Flux is the democratization of metabolic fluxes.

Methods

Generation of metabolic models

Five metabolic models were designed for the simulation of isotope labeling patterns and training for ML-Flux: 1) a simplified upper glycolysis and the PPP, 2) upper glycolysis 3) full glycolysis, 4) glycolysis and the PPP, and 5) mammalian CCM. All models contained one input metabolite (A or glucose) except for the CCM model, which also included glutamine as an input metabolite. All intracellular reactions in each metabolic model contained net and exchange fluxes to reflect that enzyme-catalyzed reactions are reversible with forward and reverse components. Physiologically relevant direction and reversibility were defined as linear equality and inequality constraints. Metabolic models were constructed and coded in an Extensible Markup Language (XML) format for simple and standardized archiving and sharing. Reactions considered in each model are detailed in **Fig. 1c**, **Fig. 2a** and **Supplemental Tables 2-5**.

Analytical solutions to simple metabolic models

In simple metabolic models, analytical solutions to fluxes as a function of labeling can be determined by applying metabolic steady-state mass balance to all metabolite levels in the model as well isotopic steady-state mass balance to all isotopologues for a given isotope tracer experiment. Metabolic steady state is defined as:

$$\boldsymbol{Sv} = \mathbf{0}$$

$\boldsymbol{S}$ is the stoichiometric matrix with rows and columns representing metabolites and reactions. $\boldsymbol{v}$ is the vector of fluxes for each reaction in $\boldsymbol{S}$.

Isotopologue mass balance relates the MID measurements to fluxes. In the simple model using the [1-$^{13}C_1$]-A tracer, balances on B_{M+1} and D_{M+1} are all that are necessary to obtain fluxes for the whole system.

$$\frac{dB_1}{dt} = 0 = v_1 - (v_{2f} + v_3 + v_4)B_{M+1} + v_{2r}D_{M+1}$$

$$\frac{dD_1}{dt} = 0 = v_{2f}B_{M+1} - (v_{2r} + v_5)\, D_{M+1}$$

These equations can be rearranged, with all fluxes being represented only by three linearly independent fluxes. By normalizing all reaction fluxes to that of aa reference reaction (i.e., v_1=1 in this example), the analytical solutions to v_3 and v_{2r} can be derived.

Sampling of metabolic fluxes

Fluxes for simulation of metabolite labeling patterns were randomly sampled within physiologically relevant flux space (**Supplemental Tables 2-5**). At metabolic steady state, the net fluxes of the system reside in the null space of **S**. Free net fluxes can be found from its reduced row echelon form using the rank-nullity theorem, and the multiplication of the basis of the null space by free net fluxes returns the full set of net fluxes. All exchange fluxes are free variables. Free net fluxes were generated using a linearly uniform random distribution. Exchange fluxes were generated using either a linearly uniform, logarithmically uniform, or logarithmically normal random distribution. If a randomly generated set of net and exchange fluxes fell within specified linear constraints, it was accepted into the training dataset. An additional sampling method included accepting flux sets based on a data density normalization so that simulated labeling patterns are uniformly distributed. For each set of fluxes, the average Euclidean distance to the 10 nearest already accepted points was recorded (D_i). The proportion of accepted flux sets with a smaller D

was determined as the probability of acceptance. For the simple, upper glycolysis, and full glycolysis models, 100,000 flux sets were generated. 1,000,000 flux sets were generated in the glycolysis+PPP model. 1,200,000 flux sets were generated for the CCM model.

Simulation of isotope labeling patterns

For each flux set, metabolite metabolite labeling patterns were simulated starting from various isotope tracers. For the simple model, all possible tracer forms of metabolite A were used for simulation except for the trivial set (i.e., fully labeled or fully unlabeled). For upper and full glycolysis models, [1,2-$^{13}C_2$]-glucose and [5-$^{2}H_1$]-glucose tracers were used. In the glycolysis+PPP model, the 24 commercially available ^{13}C-glucose tracers were used. In the CCM model, the 10 most cited ^{13}C-glucose tracers as found on Google Scholar were simulated with a combination of either unlabeled or [U-$^{13}C_5$]-glutamine for a total of 20 unique tracer combinations. Isotope labeling patterns were simulated following the EMU approach[11]. Models in an XML format[34] with atom mapping information were processed through MATLAB scripts to reconstruct them as **S** and EMU networks. Using the sampled free net and exchange fluxes, the EMU framework was employed to find the minimum isotopologue conversion networks and simulate isotopic labeling fractions based on the atom mapping across reactions. The resulting pairs of reaction fluxes and metabolite labeling patterns were stored in .dat files. Files were formatted such that each row contained labeling data for a single simulation, ordered by metabolite, the isotope tracer used, and then labeling isotopologue.

Flux prediction by artificial neural network models

Simulated flux-to-label simulations were used to train five unique fully connected feedforward ANNs. The input layer for each of these ANNs was the complete isotope labeling information of every metabolite within the metabolic model for every isotope tracer used. The output layer contained only the free fluxes of the metabolic model. Training only under the set of free fluxes ensures that the minimal linearly independent output nodes are used, and the resulting full flux set is always mass balanced.

Simulated data were split into training, validation, and testing at a ratio of 0.8:0.1:0.1. ANN training scripts were written in Python using the Keras library. Prior to training, fluxes were transformed under a piecewise logistic or logarithmic function to minimize the effect of very large fluxes (**Extended Data Figure 2b**). Inputs for neural networks thus were the metabolite labeling patterns, and the output was transformed free fluxes, which were later reverted to the actual values by inverse functions. Each neural network contained one input layer for MIDs, five hidden layers, and one output layer for free fluxes. The number of nodes within each hidden layer was chosen empirically in each ANN depending on the complexity of the metabolic models. With the exception of the single-tracer simple model, all training was conducted on the UCLA Hoffman2 Cluster.

Imputation of labeling data by KNN-regression and partial convolutional neural networks

Simulated labeling data ere were masked to emulate the proportion of incomplete information due to an inability to detect a subset of metabolites or perform a subset of isotope tracer experiments (**Supplemental Table 6**). As researchers typically conduct one tracer experiment, we generated masks that removed labeling data from all but one isotope tracer. Furthermore, metabolites within the model were randomly masked to emulate situations where not every metabolite is measured. Imputation of labeling data via KNN-regression was performed using the scikit-learn library, with incomplete-complete matrix pairs were split into training, validation, and testing at ratio of 0.8:0.1:0.1. The nearest K=3 neighbors by

Euclidean distance was used to compute missing labeling values, with the influence of each neighbor on the prediction weighted by its distance.

The same masked labeling data were used for inpainting model training by PCNN using the Keras library. The labeling data were reshaped into a rectangular matrix and overlaid on the center of a square matrix. The extra space was padded with ones and not masked. The size of the square matrix ranged from 16x16 to 80x80 depending on the size of metabolic networks. 100,000 metabolite labeling sets were used as original matrices for training. 500 random masks for the simple, upper glycolysis, and glycolysis models were generated for each complete metabolite labeling matrix, while 4,000 masks were generated each for the glycolysis+PPP and CCM models. The incomplete-complete matrix pairs were split into training, validation, and testing at ratio of 0.8:0.1:0.1. Mean absolute error (MAE) or mean squared error (MSE) was used for the loss function. The choice of MAE or MSE depended on the metabolic network. We found the CCM network could achieve better ΔN values using the MSE loss function. PCNN-based inpainting training was conducted using A100 GPU nodes on the Anvil cluster at Purdue.

The plausibility of inpainted MID matrix was quantified by the following equation (near-zero ΔN values indicate high plausibility of inpainted labeling patterns):

$$\Delta N = \sum_{i=1}^{I} \sum_{m=1}^{M} \sum_{n=0}^{N} f_{i,m,n} - M \cdot I$$

Here, *i* represents an isotope tracer experiment simulated in the model, *m* represents a metabolite in the pathway model, *n* represents a mass isotopomer M+n, and $f_{i,m,n}$ represents the fraction of M+n isotopomer of metabolite m given an isotope tracer *i*. *M* is the total number of metabolites in the metabolic model, *I* is the total number of isotope tracers used for training ML models, and *N* is the maximum number of atoms considered in atom mapping in a metabolite.

Accuracy score for predicting pathway fluxes

ML-Flux predictions of the fluxes in CCM from experimental were compared to MFA predictions when using seven different combinations of isotope tracers. An accuracy score for each tracer combination was defined to compare between tracer combinations:

$$Accuracy\ score = \sum_i R_i$$

R represents the rank (out of the seven tracers) of how close this tracer combination's prediction of flux *i* was to that of the MFA determined value. An R_i of seven represents the closest combination, while a value of one represents the least accurate tracer combination for that flux. Thus, a high accuracy score corresponds to an ability to a good prediction of the flux set in a given system.

Online deployment of ML-Flux

All machine learning model architectures were stored in .json files with accompanying weights and biases in .h5 files. Reading these files for model prediction requires minimal software, enabling light deployment onto a website using a Python backend and the Bootstrap CSS framework. We provide a detailed documentation with examples and template input files on metabolicflux.org.

Data Availability

All data are available on the GitHub public repository: https://github.com/richardlaw517/ML-Flux

Code Availability

The code for simulating isotope labeling data and training machine learning models is available on the GitHub public repository: https://github.com/richardlaw517/ML-Flux

The code for ML-Flux website is available on the GitHub public repository: https://github.com/richardlaw517/ML-Flux

Acknowledgements

The authors would like to thank the members of the Park lab, UCLA Metabolomics Center, and UCLA Molecular Instrumentation Center for constructive feedback. This work was supported by the National Institute of General Medical Sciences of the National Institutes of Health under Award Number R35GM143127 (J.O.P.), the Department of Energy under Award Number DE-SC0024251 (J.O.P. and P.K.L.), the Center for Clean Technology Fellowship (R.C.L.), the National Science Foundation Research Traineeship in Integrated Urban Solutions for Food, Energy, and Water Management (NSF-INFEWS) under Award Number DGE-1735325 (G.N.), the BioPACIFIC Materials Innovation Platform of the National Science Foundation under Award Number DMR-1933487 (R.C.L., G.N., and J.O.P.), and the National Institutes of Health Biotechnology Training Grant under Award Number T32GM067555 (A.L.). This work used computational and storage services associated with the Hoffman2 Shared Cluster provided by UCLA Institute for Digital Research and Education's Research Technology Group as well as the Advanced Cyberinfrastructure Coordination Ecosystem: Services & Support (ACCESS) computing resources (CHM230023). The content is solely the responsibility of the authors and does not necessarily represent the official views of the National Institutes of Health, the Department of Energy, or the National Science Foundation.

Author Contributions

R.C.L., P.K.L., and J.O.P. designed the study. R.C.L, S.O., G.N., and J.O.P. generated the metabolic models. R.C.L., S.O., and G.N. generated flux-to-labeling simulation datasets. R.C.L. and P.K.L. designed, trained, validated, and tested machine learning models. R.C.L. integrated metabolic and machine learning models and generated the final Python scripts for ML-Flux prediction. R.C.L., R.K., and J.O.P. created the web interface for ML-Flux. R.K. and R.C.L. wrote the operational manual for ML-Flux. R.C.L. and J.O.P. wrote the manuscript with input from all the authors.

Competing Interests

The authors declare no competing financial or non-financial interests.

References

1. Park, J. O. *et al.* Near-equilibrium glycolysis supports metabolic homeostasis and energy yield. *Nature Chemical Biology 2019 15:10* **15**, 1001–1008 (2019).

2. Karp, P. D. *et al.* The BioCyc collection of microbial genomes and metabolic pathways. *Brief Bioinform* **20**, 1085–1093 (2019).

3. King, Z. A. *et al.* BiGG Models: A platform for integrating, standardizing and sharing genome-scale models. *Nucleic Acids Res* **44**, D515–D522 (2016).

4. Kanehisa, M. & Goto, S. KEGG: kyoto encyclopedia of genes and genomes. *Nucleic Acids Res* **28**, 27–30 (2000).

5. Perez de Souza, L., Alseekh, S., Scossa, F. & Fernie, A. R. Ultra-high-performance liquid chromatography high-resolution mass spectrometry variants for metabolomics research. *Nature Methods 2021 18:7* **18**, 733–746 (2021).

6. Emwas, A. H. *et al.* NMR Spectroscopy for Metabolomics Research. *Metabolites 2019, Vol. 9, Page 123* **9**, 123 (2019).

7. Hackett, S. R. *et al.* Systems-level analysis of mechanisms regulating yeast metabolic flux. *Science (1979)* **354**, (2016).

8. Liebermeister, W. & Klipp, E. Bringing metabolic networks to life: convenience rate law and thermodynamic constraints. *Theor Biol Med Model* **3**, 41 (2006).

9. Heirendt, L. *et al.* Creation and analysis of biochemical constraint-based models using the COBRA Toolbox v.3.0. *Nature Protocols 2019 14:3* **14**, 639–702 (2019).

10. Law, R. C., Lakhani, A., O'Keeffe, S., Erşan, S. & Park, J. O. Integrative metabolic flux analysis reveals an indispensable dimension of phenotypes. *Curr Opin Biotechnol* **75**, 102701 (2022).

11. Antoniewicz, M. R., Kelleher, J. K. & Stephanopoulos, G. Elementary metabolite units (EMU): A novel framework for modeling isotopic distributions. *Metab Eng* **9**, 68–86 (2007).

12. Young, J. D., Walther, J. L., Antoniewicz, M. R., Yoo, H. & Stephanopoulos, G. An elementary metabolite unit (EMU) based method of isotopically nonstationary flux analysis. *Biotechnol Bioeng* **99**, 686–699 (2008).

13. Wiechert, W., Möllney, M., Petersen, S. & De Graaf, A. A. A Universal Framework for 13C Metabolic Flux Analysis. *Metab Eng* **3**, 265–283 (2001).

14. Wiechert, W., Mö, M., Isermann, N., Wurzel, M. & De Graaf, A. A. Bidirectional Reaction Steps in Metabolic Networks: III. Explicit Solution and Analysis of Isotopomer Labeling Systems. *& Sons, Inc. Biotechnol Bioeng* **66**, 69–85 (1999).

15. Buescher, J. M. *et al.* A roadmap for interpreting 13C metabolite labeling patterns from cells. *Curr Opin Biotechnol* **34**, 189–201 (2015).

16. Wishart, D. S. NMR metabolomics: A look ahead. *Journal of Magnetic Resonance* **306**, 155–161 (2019).

449 17. Alseekh, S. *et al.* Mass spectrometry-based metabolomics: a guide for annotation, quantification and best
450 reporting practices. *Nature Methods 2021 18:7* **18**, 747–756 (2021).

451 18. Tang, Y. J. *et al.* Advances in analysis of microbial metabolic fluxes via 13C isotopic labeling. *Mass*
452 *Spectrom Rev* **28**, 362–375 (2009).

453 19. Rahim, M. *et al.* INCA 2.0: A tool for integrated, dynamic modeling of NMR- and MS-based isotopomer
454 measurements and rigorous metabolic flux analysis. *Metab Eng* **69**, 275–285 (2022).

455 20. Shupletsov, M. S. *et al.* OpenFLUX2: (13)C-MFA modeling software package adjusted for the
456 comprehensive analysis of single and parallel labeling experiments. *Microb Cell Fact* **13**, (2014).

457 21. Weitzel, M. *et al.* 13CFLUX2—high-performance software suite for 13C-metabolic flux analysis.
458 *Bioinformatics* **29**, 143–145 (2013).

459 22. Yoo, H., Antoniewicz, M. R., Stephanopoulos, G. & Kelleher, J. K. Quantifying Reductive Carboxylation Flux
460 of Glutamine to Lipid in a Brown Adipocyte Cell Line. *Journal of Biological Chemistry* **283**, 20621–20627
461 (2008).

462 23. Abiodun, O. I. *et al.* State-of-the-art in artificial neural network applications: A survey. *Heliyon* **4**, (2018).

463 24. Liu, G. *et al.* Image Inpainting for Irregular Holes Using Partial Convolutions.

464 25. Crown, S. B. & Antoniewicz, M. R. Selection of tracers for 13C-Metabolic Flux Analysis using Elementary
465 Metabolite Units (EMU) basis vector methodology. *Metab Eng* **14**, 150–161 (2012).

466 26. Crown, S. B., Long, C. P. & Antoniewicz, M. R. Optimal tracers for parallel labeling experiments and 13C
467 metabolic flux analysis: A new precision and synergy scoring system. *Metab Eng* **38**, 10–18 (2016).

468 27. Antoniewicz, M. R. Parallel labeling experiments for pathway elucidation and 13C metabolic flux analysis.
469 *Curr Opin Biotechnol* **36**, 91–97 (2015).

470 28. Park, J. O. *et al.* Metabolite concentrations, fluxes and free energies imply efficient enzyme usage. *Nature*
471 *Chemical Biology 2016 12:7* **12**, 482–489 (2016).

472 29. Hackett, S. R. *et al.* Systems-level analysis of mechanisms regulating yeast metabolic flux. *Science (1979)*
473 **354**, (2016).

474 30. Shlomi, T., Cabili, M. N., Herrgård, M. J., Palsson, B. & Ruppin, E. Network-based prediction of human
475 tissue-specific metabolism. *Nature Biotechnology 2008 26:9* **26**, 1003–1010 (2008).

476 31. Hui, S. *et al.* Quantitative proteomic analysis reveals a simple strategy of global resource allocation in
477 bacteria. *Mol Syst Biol* **11**, 784 (2015).

478 32. Buescher, J. M. *et al.* A roadmap for interpreting 13C metabolite labeling patterns from cells. *Curr Opin*
479 *Biotechnol* **34**, 189–201 (2015).

480 33. Beard, D. A. & Qian, H. Relationship between Thermodynamic Driving Force and One-Way Fluxes in
481 Reversible Processes. *PLoS One* **2**, e144 (2007).

482 34. Weitzel, M. *et al.* 13CFLUX2—high-performance software suite for 13C-metabolic flux analysis.
483 *Bioinformatics* **29**, 143 (2013).

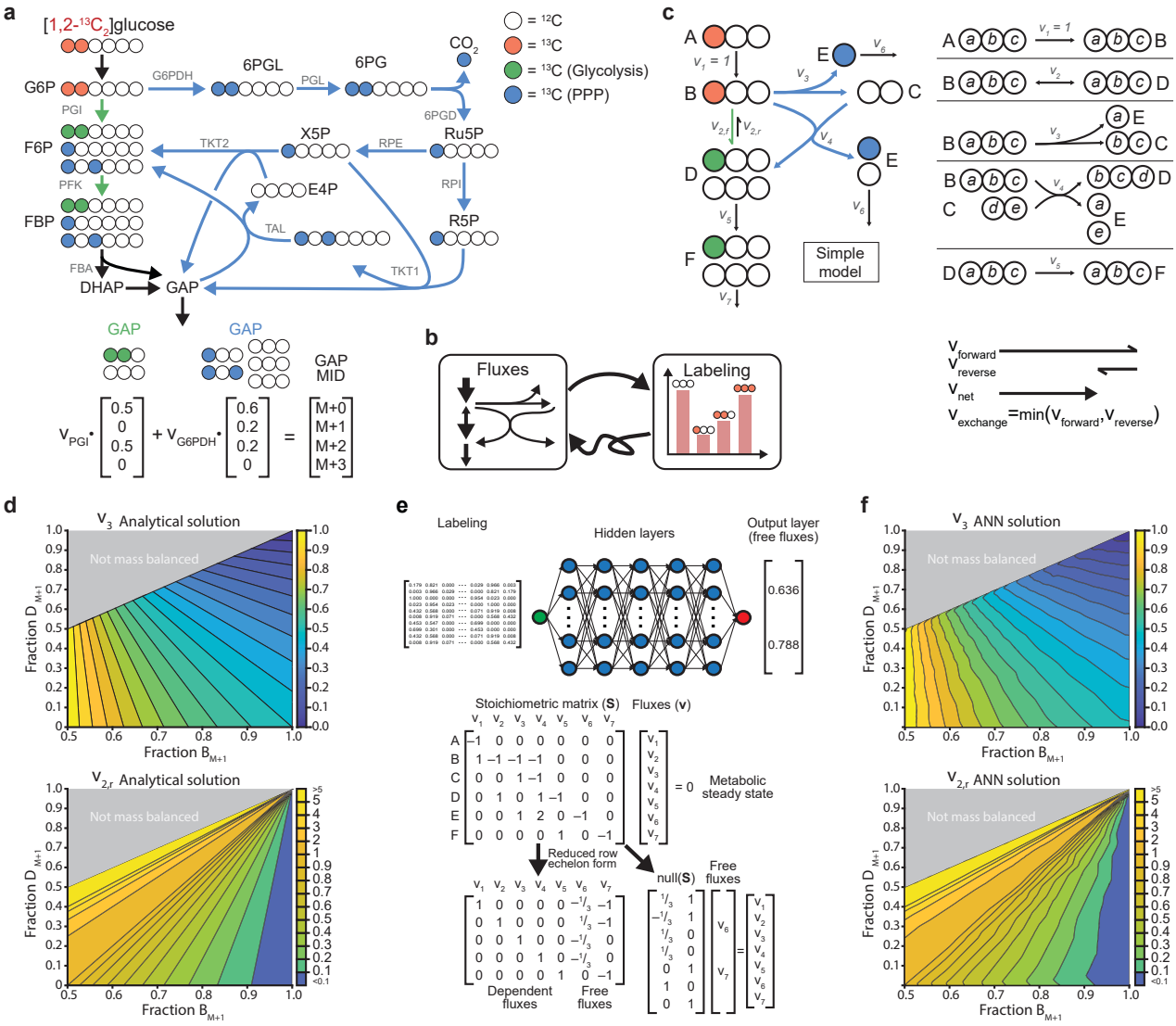

Figure 1: Isotope tracers generate isotopologues that correspond to metabolic fluxes

a, Tracing [1,2-$^{13}C_2$]-glucose discerns relative usage of glycolysis and the pentose phosphate pathway (PPP). The mass isotopomer distribution (MID) of the convergent product glyceraldehyde-3-phosphate (GAP) is a linear combination of pathway-specific isotopologues weighted by pathway fluxes. **b,** Simulation metabolite labeling patterns (i.e., MID) from an isotope tracer given fluxes is a straightforward process, but the process of quantifying fluxes given MID is convoluted and indirect. **c,** A simplified model of glycolysis and PPP illustrates how atomic transitions impact labeling. Feeding [1-$^{13}C_1$]-A into the system results in unique labeling patterns as a function of v_3. The addition of a reverse flux $v_{2,r}$ introduces unlabeled B. **d,** Analytical solutions for v_3 and $v_{2,r}$, which are free fluxes in the model, were solved as functions of B and D labeling. Each axis represents the fractional labeling of the singly labeled (M+1) isotopomer, while the color scale represents the flux value. **e,** An artificial neural network (ANN) can be trained to take labeling data as input and predict v_3 and $v_{2,r}$ as output. The remaining dependent fluxes can be calculated as a linear combination of the free fluxes. **f,** An ANN model was trained from pairs of fluxes and simulated metabolite labeling patterns.

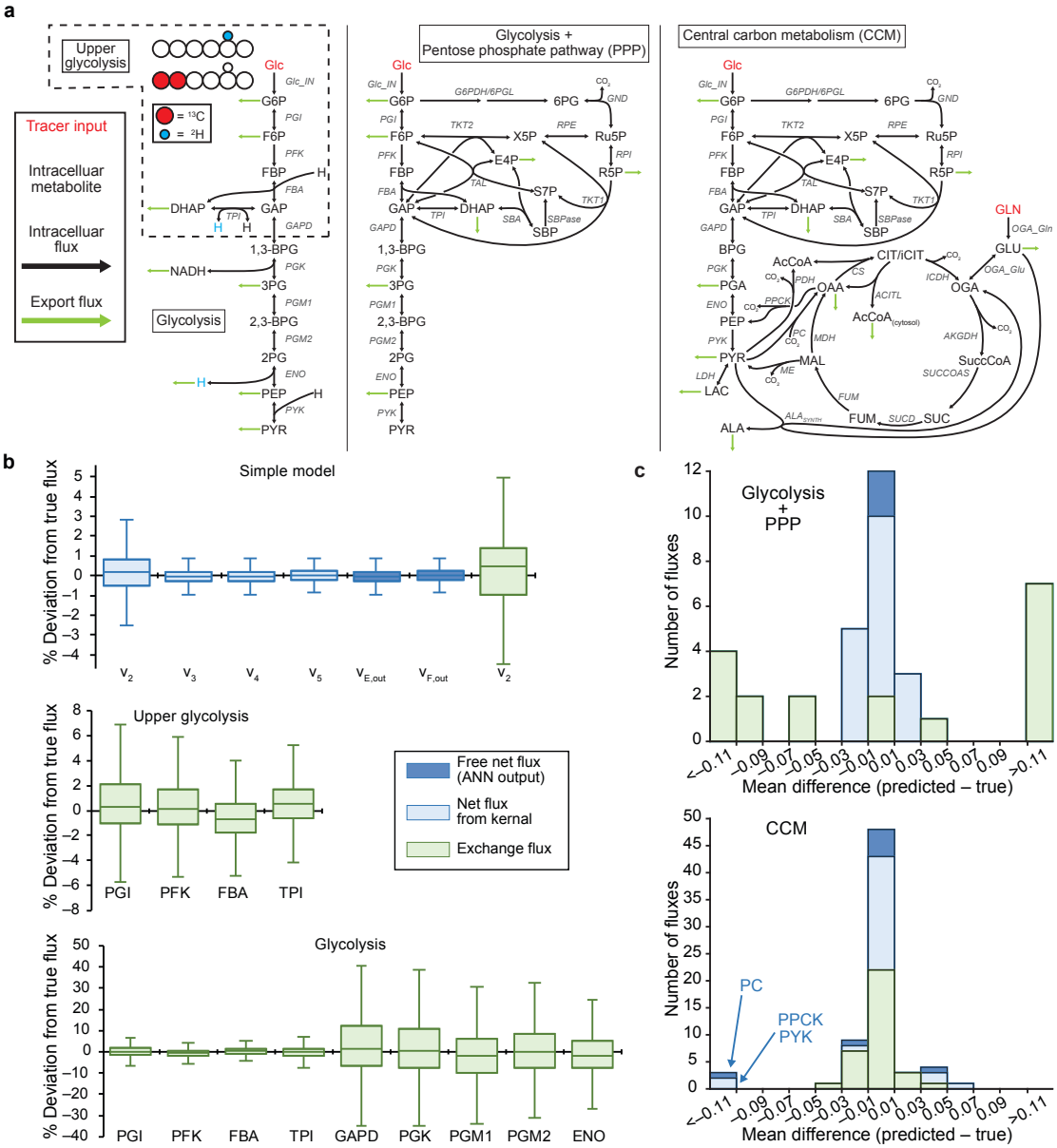

Figure 2: Artificial neural networks decipher the relationship between metabolite labeling and flux

a, ANNs were trained to predict fluxes in four models of central carbon metabolism at different scopes. Each metabolic network was used to simulate labeling data from randomly sampled fluxes. The resulting datasets were used to train, validate, and test the ANN models for the prediction of fluxes in the respective metabolic networks. **b,** Free net (dark blue) and exchange (green) fluxes were predicted from testing data for each metabolic model. The remaining dependent net fluxes (light blue) were computed from the free net fluxes. The distribution of errors associated with flux predictions are reported for the simple, upper glycolysis, and glycolysis models. Each box shows the three quartiles, and whiskers extend to the minimum and maximum values within 1.5-fold of the interquartile range (n = 10,000 test data points). **c,** The mean difference of all test predictions for each flux was computed for the glycolysis+PPP and CCM models (n = 100,000 test data points).

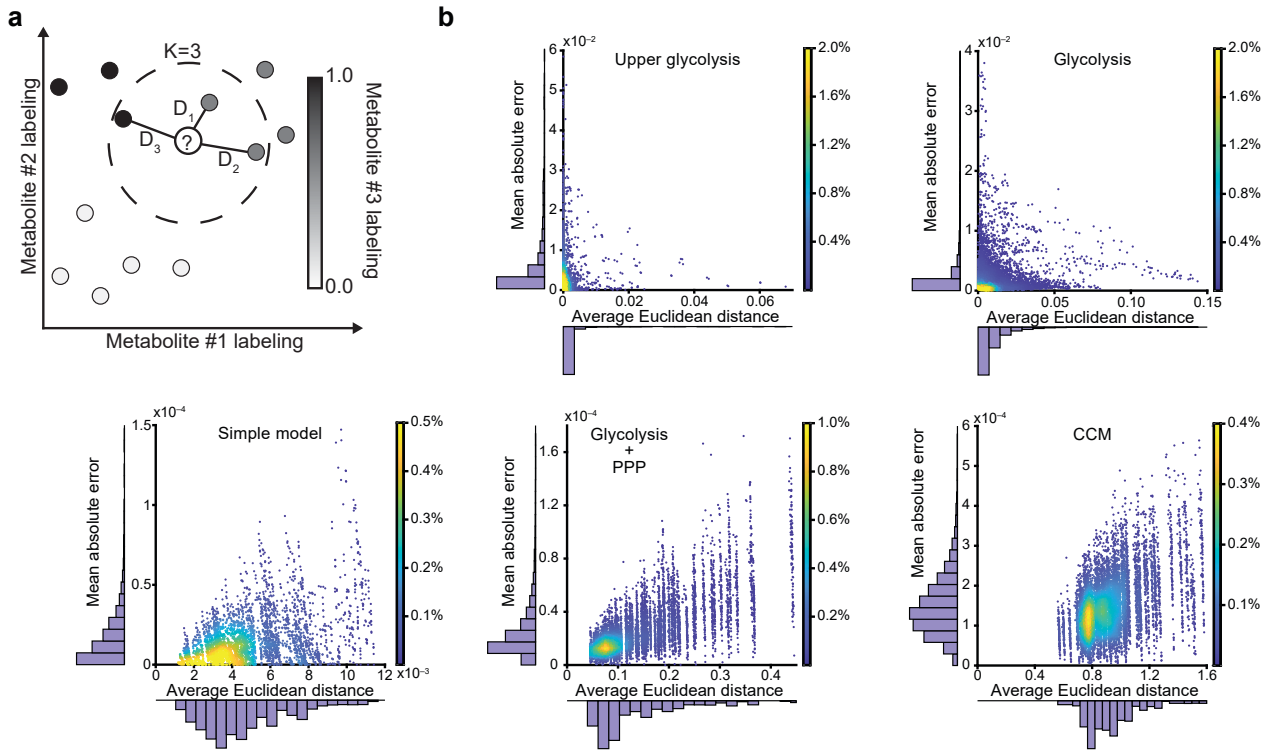

Figure 3: K-nearest neighbors regression imputes variably incomplete labeling information

a, In K-nearest neighbors (KNN) regression, known values of an incomplete labeling set is compared to training data that is complete (i.e., the labeling patterns of all metabolites are known) to identify the K (three in this case) similar labeling points by Euclidean distance. The unknown values are imputed as the weighted mean of the corresponding known labeling of the nearest neighbors. **b,** For each metabolic network, randomly generated masks partially covered each of 100 complete labeling patterns to hide data corresponding to a subset of metabolites and tracer experiments. These masked datasets were imputed with KNN regression. The mean absolute errors of predicted labeling patterns were compared to the average Euclidean distance to three neighbors.

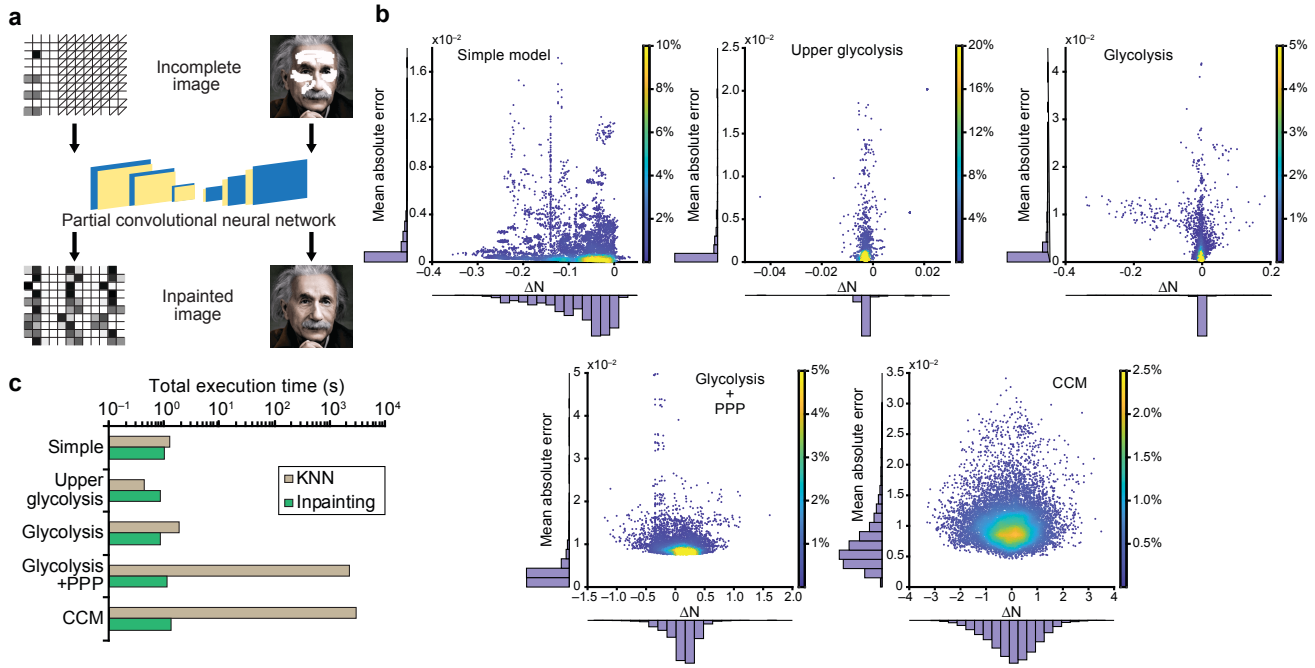

Figure 4: Deep-learning-based inpainting rapidly imputes variably incomplete labeling information

a, Labeling data in a matrix form are similar to pixels in a black-and-white image. Missing 'pixels' in labeling data may be predicted by training a partial convolutional neural network (PCNN) similar to how various missing portions of an image are restored from inpainting. **b,** For each metabolic network, randomly generated masks partially covered each of 100 complete labeling patterns to hide data corresponding to a subset of metabolites and tracer experiments. PCNN models were trained using the masked and unmasked datasets. The mean absolute errors of predicted labeling patterns were compared to the difference between the grand sum of the inpainted MID matrix and the total number of measured metabolite instances (ΔN). Values of ΔN near zero indicate high plausibility of inpainted labeling patterns. **c,** The speeds of KNN regression and inpainting were benchmarked by their total execution time to impute one set of incomplete labeling information.

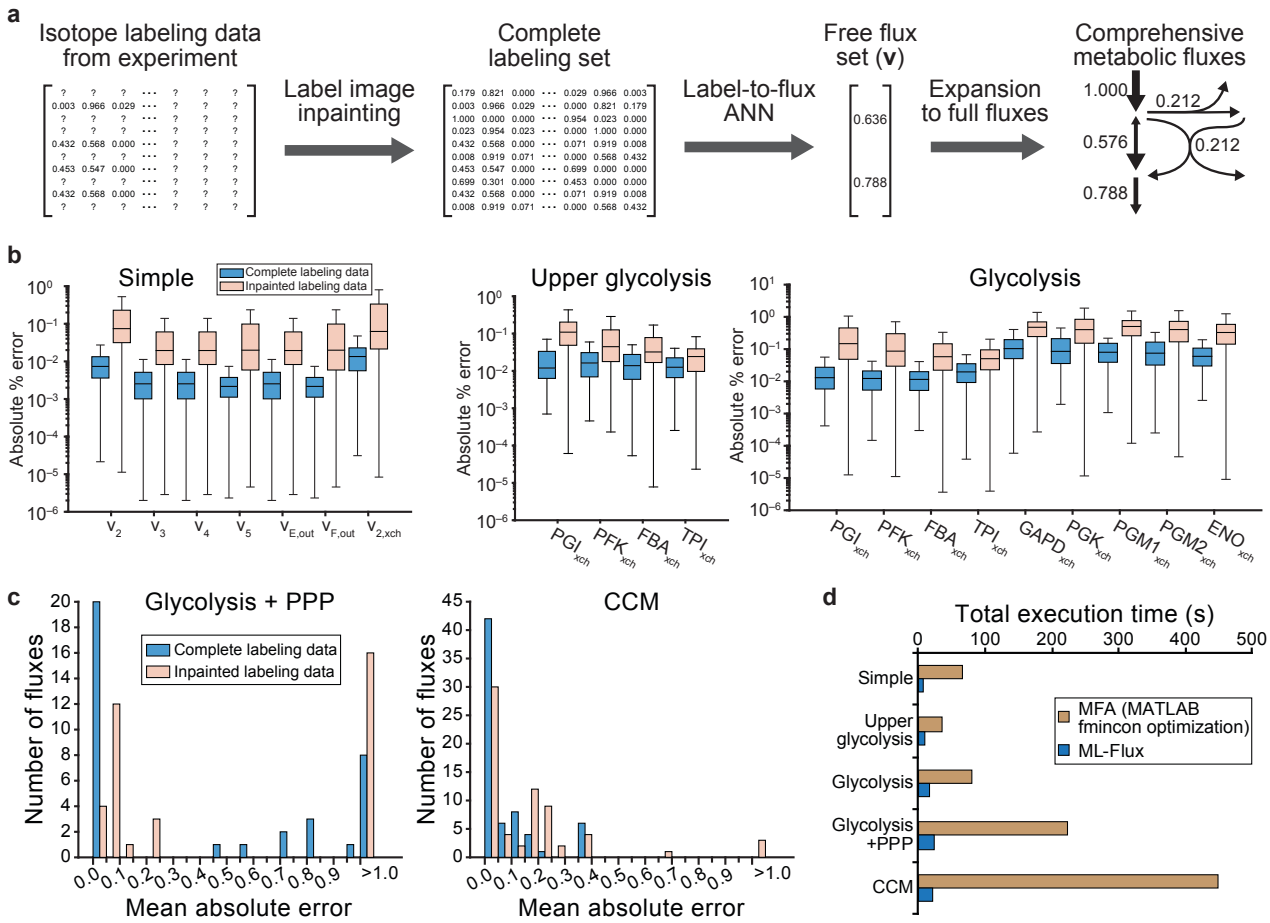

Figure 5: Integrated ML models produce accurate fluxes from limited labeling data

a, PCNN imputation and ANN flux prediction were integrated to convert variable measurement of metabolite labeling patterns into free fluxes, which were expanded to a comprehensive flux map using linear algebra. **b,** Fluxes were predicted either from complete labeling information or masked versions of the same data after the PCNN imputation. The distribution of their absolute percent errors was plotted for the simple, upper glycolysis, and glycolysis models. Each box shows the three quartiles, and whiskers extend to the minimum and maximum values within 1.5-fold of the interquartile range (n = 100 test data points for complete labeling data and n=10,000 for simple and glycolysis masked labeling data and n=3,100 for upper glycolysis masked labeling data). **c,** The distributions of mean absolute errors of fluxes Glycolysis + PPP and CCM were plotted for complete and inpainted labeling patterns. **d,** Total execution times for flux prediction were measured in the ML-Flux, with the PCNN-ANN integration, and least squares MFA software across different metabolic models.

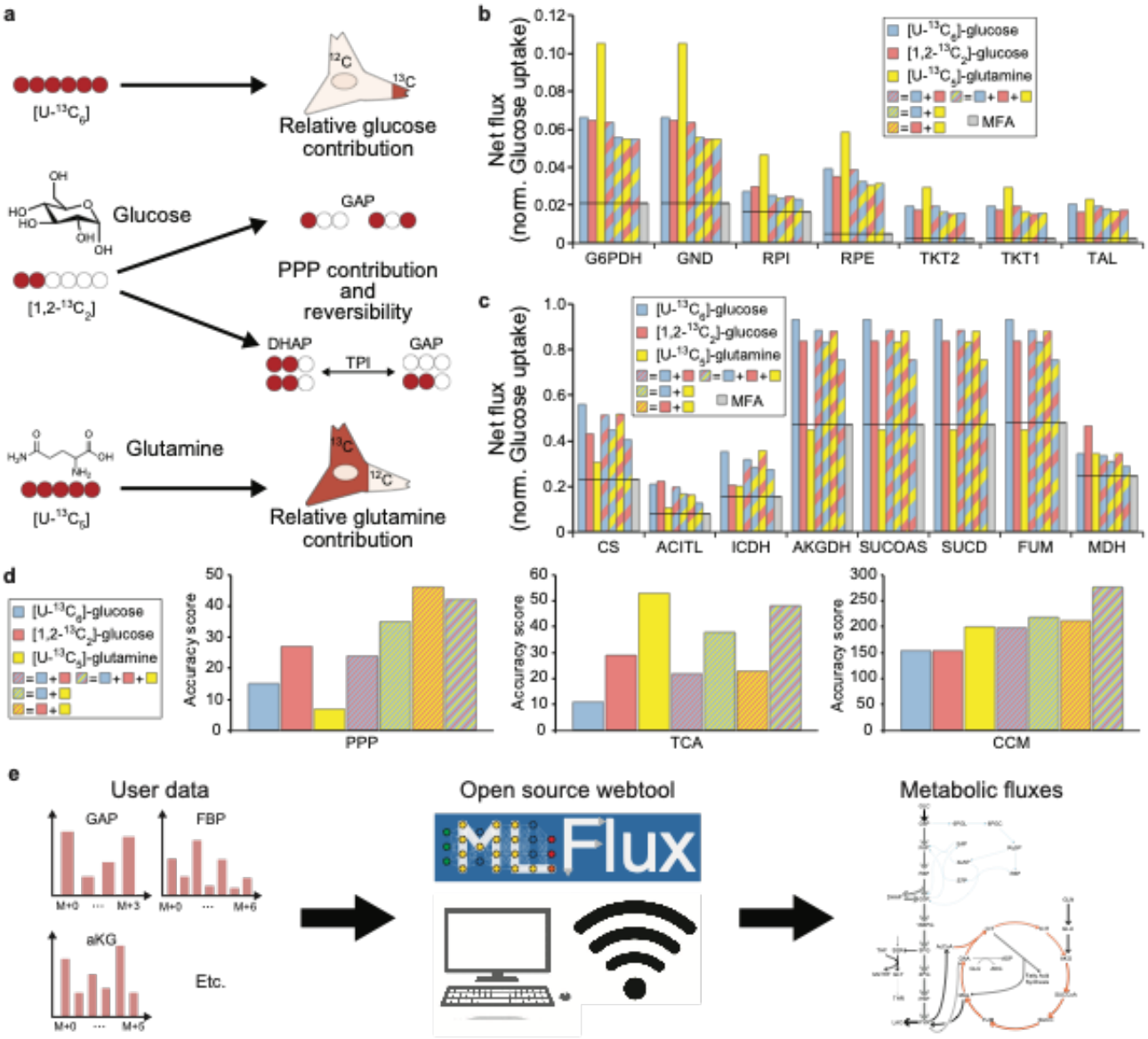

Figure 6: ML-Flux computes fluxes from multi-isotope tracing experiments

a, Different tracers impart flux information on different metabolic pathways. Metabolite labeling in cells fed with [U-$^{13}C_6$]-glucose reveals the contribution of glucose to pathways such as the TCA cycle, to which multiple nutrients contribute. Similarly, [U-$^{13}C_5$]-glutamine reveals the contribution of glutamine to the TCA cycle. [1,2-$^{13}C_2$]-glucose tracing reveals fluxes in the PPP and reversibility of upper glycolysis and PPP reactions. **b,** Net fluxes in PPP were predicted using ML-Flux with various combinations labeling measurements from [U-$^{13}C_6$]-glucose, [1,2-$^{13}C_2$]-glucose, and/or [U-$^{13}C_5$]-glutamine tracers. Predicted fluxes were compared to ^{13}C-MFA conducted using all three tracers together. **c**, Net fluxes in the TCA cycle were predicted using the same tracer configurations and compared to results from ^{13}C-MFA. **d,** The accuracy scores were computed by ranking flux predictions from different tracer combinations by their proximity to the MFA predicted values for the subsets (i.e., the PPP and the TCA cycle) and the full set of CCM reactions. **e,** ML-Flux was implemented in a website for quick and easy flux analysis.

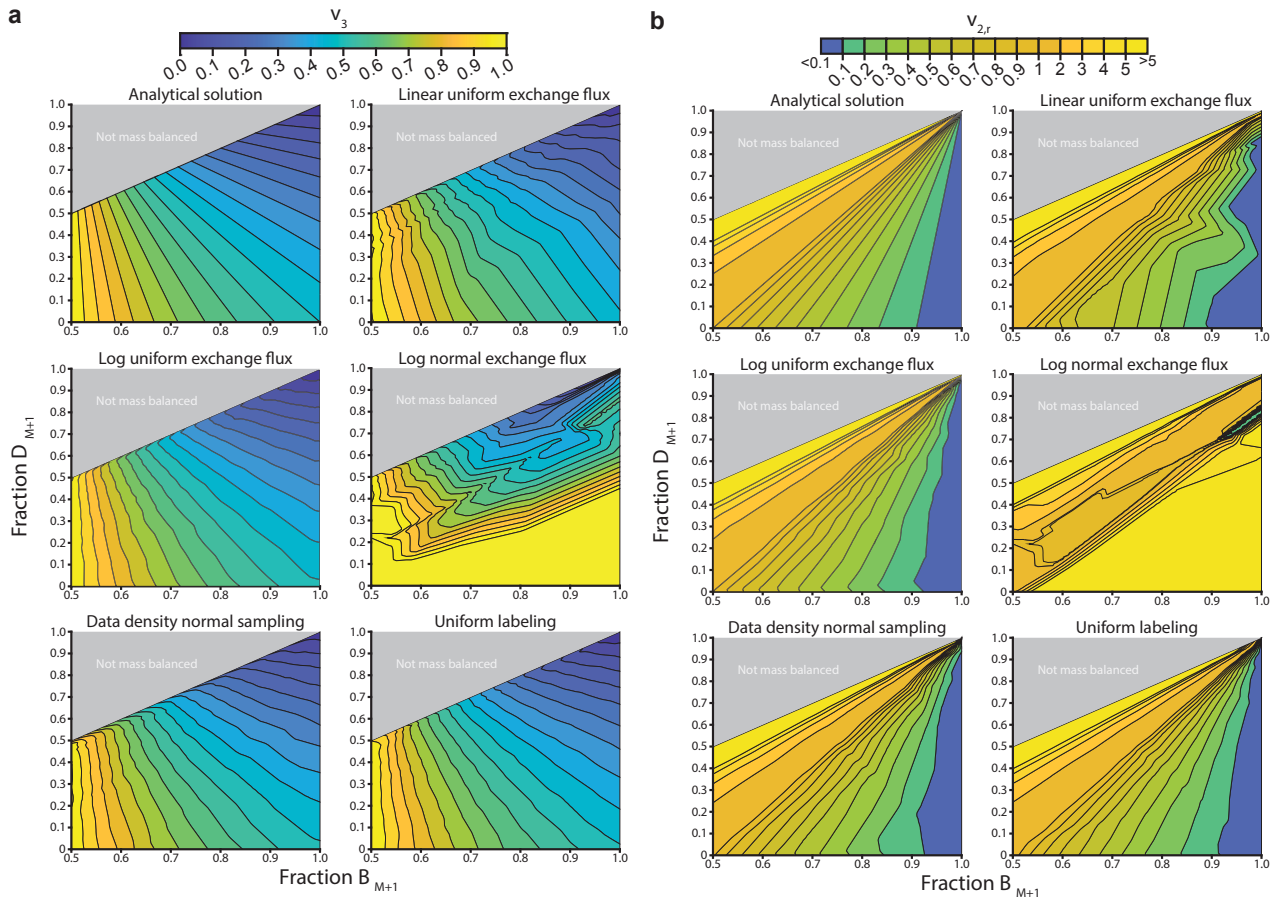

Extended Data Figure 1: Different flux sampling methods to generate training datasets alter the outcome of ANN model training

a and **b,** Five different sampling approaches for generating flux-to-label simulations for training were tested and compared to the analytical solution (top left) for v_3 (**a**) and $v_{2,r}$ (**b**) (see **Methods**). Each panel shows the solution space for v_3 or $v_{2,r}$ using one of the sampling approaches.

a

	Simple	Upper glycolysis	Glycolysis	Glycolysis + PPP	CCM
Size of input (labeling)	120	25	192	3,456	4,800
Size of output (transformed free fluxes)	6	7	18	33	55
Number of hidden layers	5				
Number of trainable parameters	2871	14,199	149,717	17,191,592	44,437,765
Dataset size	100,000	100,000	100,000	1,000,000	1,200,000
Number of epochs trained	1,000	2,000	2,000	500	500

b

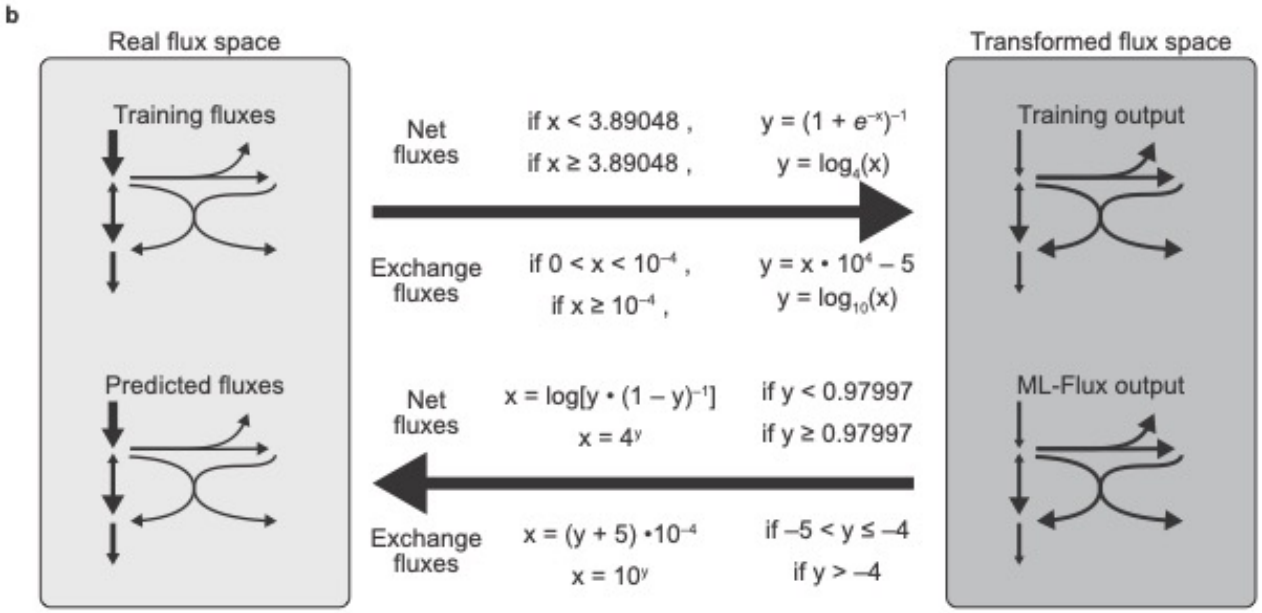

Extended Data Figure 2: Metabolite labeling patterns give rise to metabolic fluxes using ANN

a, Each metabolic model required its own ANN, with a different set of hyperparameters. **b,** To reduce bias toward training for extremely large or small fluxes, free net and exchange fluxes were transformed before being fed for training. Trained ANNs predict transformed fluxes, which are converted back into real values.

	Simple	Upper glycolysis	Glycolysis	Glycolysis + PPP	CCM
Size of input (incomplete labeling)	Variable	Variable	Variable	Variable	Variable
Size of output (complete labeling)	120	35	192	3,456	4,800
Number of trainable parameters	392,000	96,493	384,205	1,565,197	1,565,197
Number of complete labelings in dataset	100,000	100,000	100,000	1,000,000	1,000,000
Number of masks per labeling set	500	500	500	4,000	4,000
Number of epochs trained	5	5	5	1	1

Extended Data Figure 3: Hyperparameters for PCNN inpainting of missing labeling data

For each metabolic model, inpainting networks were trained using 100,000 complete MID matrices. For each complete MID matrix, copious masks were generated to generate partial labeling data for training, resulting in 500,000 to 4 billion unique pairs of incomplete-complete labeling data to train the PCNN models.

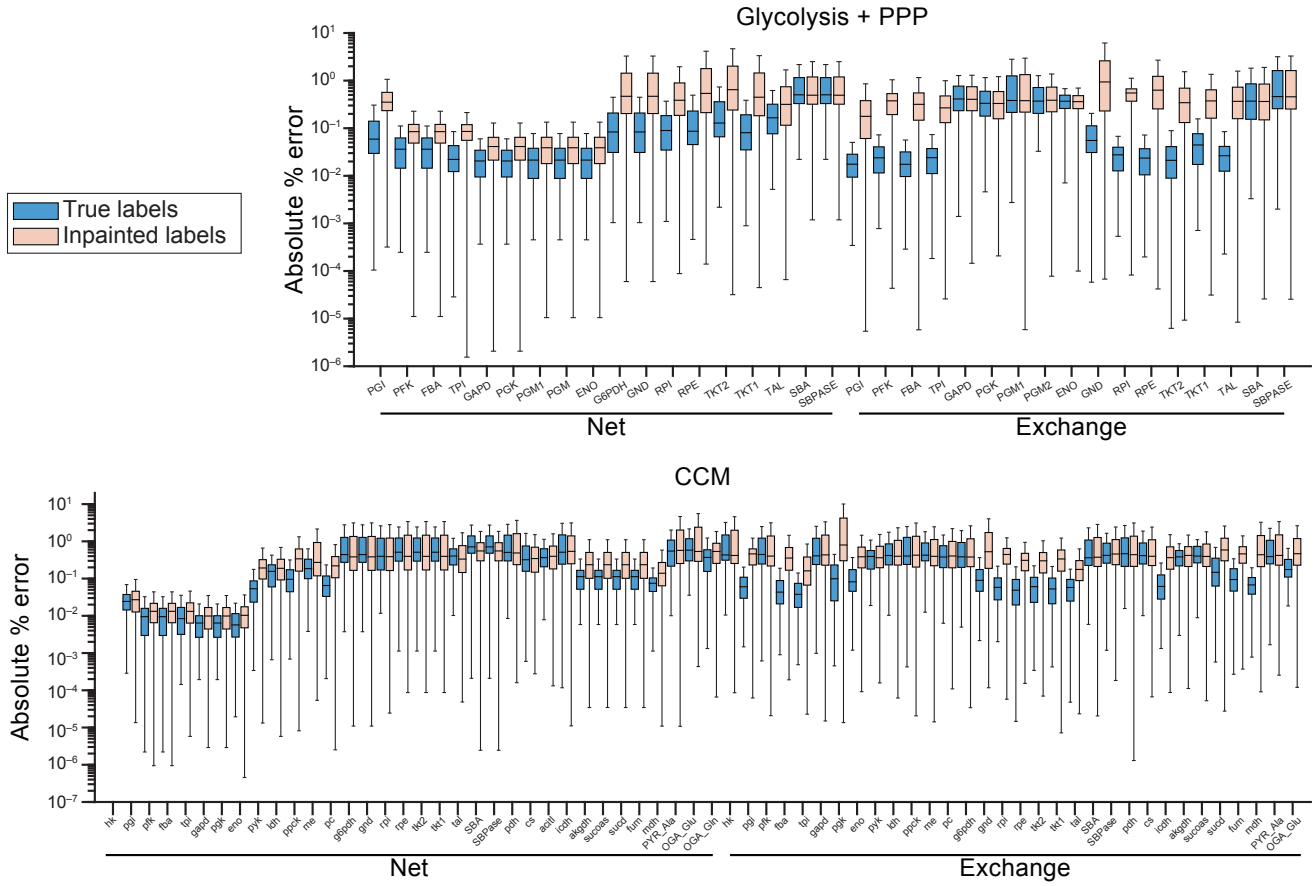

Extended Data Figure 4: Integrated ML-Flux models predict net and exchange fluxes for central carbon metabolism

Fluxes were predicted either from complete labeling datasets or masked versions of the same datasets that undergo PCNN imputation. The distribution of their absolute percent errors was measured for the glycolysis+PPP and CCM models.

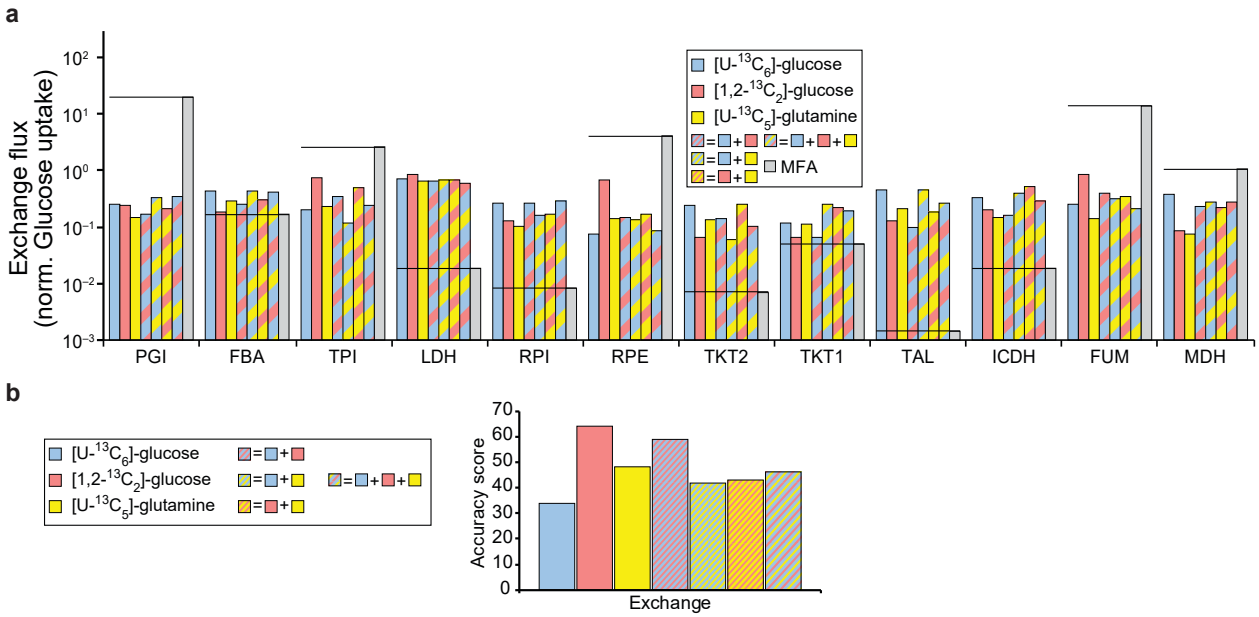

Extended Data Figure 5: Exchange flux prediction accuracy depends on the choice of tracers

a, Exchange fluxes were predicted using ML-Flux, including combinations of [U-$^{13}C_6$]-glucose, [1,2-$^{13}C_2$]-glucose, and [U-$^{13}C_5$]-glutamine tracers. Predicted fluxes were compared to those of ^{13}C-MFA fitting all three tracing datasets simultaneously. **b,** The accuracy scores were computed by ranking flux predictions from different tracer combinations by their proximity to the MFA predicted values for the exchange fluxes.